https://doi.org/10.15407/ujpe71.4.331

YU.P. GNATENKO,[1] A.P. BUKIVSKII,[1] P.M. BUKIVSKIJ,[1] S.A. ILIASH,[1]
I.G. VERTEGEL,[1] O.I. OVCHARENKO,[1] A.S. OPANASYUK,[2] R.V. GAMERNYK,[1]
M.S. FURYER [1]

[1] Institute of Physics of the Nat. Acad. of Sci. of Ukraine
(46, Prosp. Nauky, Kyiv 03028, Ukraine)
[2] Sumy State University
(116, Kharkivska Str., Sumy UA-40007, Ukraine)

STATIONARY AND TIME-RESOLVED PHOTOLUMINESCENCE OF NANOSTRUCTURED TIN SULFIDE FILMS

In this work, the optical properties, including the photoluminescence spectra and their kinetics, of thick SnS films in the orthorhombic phase with low-level microdeformation were studied. They have the composition close to the stoichiometry. Besides, these films contain a small quantity of other crystalline phases, namely, SnS, SnS_2, SnO_2 and, possibly, Sn_2S_3 phases. The study of the absorption coefficient first and second derivative spectra, i.e. the ACFD and ACSD spectra, allowed us to determine exactly the band gaps of various crystalline phases. The analysis of ACSD spectra also makes it possible to obtain information regarding the homogeneity of the investigated nanomaterials, which is very important for the optimization of their crystal and optical quality. The study of the photoluminescence spectra allowed us to obtain information regarding the energy structure of the nanostructured SnS films and the nature of their defects. Based on the photoluminescence decay kinetics measurements, the lifetime distributions for different recombination processes in SnS_2 and SnO_2 were studied. Such studies made it possible to determine the lifetimes for various recombination processes and thus obtain additional information about their nature associated with a certain type of optical transitions, which are determined by the energy of such optical transitions. It was shown that the excited-state lifetimes in the investigated films are in the nanosecond range. Thus, the results obtained may help to develop new fast-acting, efficient nanomaterials suitable for creating ecological absorber layers for solar cells based on them.

Keywords: photoluminescence, kinetics, band gap, defects, phase state, nanostructured films.

1. Introduction

The development of novel semiconductor materials for solar cell applications is one of the top priorities of modern optoelectronics. The Solar Cell Efficiency (SCE) of the different semiconductor materials was presented in Ref. [1]. Among these materials, the highest SCE values are obtained for the following materials: Si – 27.4% [2], GaAs – 29.1% [3], CIGS – 23.3% [4], CdTe – 21.0% [5], CZTSSe – 14.1% [6], dye – 11.9% [7], organic – 15.8% [8].

It should be noted that the thin films based on CdTe and CIGS compounds are widely used in solar cells as absorber layer materials. However, they have some limitations as a result of the deficiency of tellurium (Te) and indium (In) in the Earth's crust and the toxicity of cadmium (Cd) and selenium (Se). Therefore, recently, there has been a significant increase of interest in the use of novel materials that are nontoxic and have a significant presence in the earth's crust [9–15], primarily CuO and SnS. Unlike CZTSSe, they have only a few impurity phases and can be pro-

Citation: Gnatenko Yu.P., Bukivskii A.P., Bukivskij P.M., Iliash S.A., Vertegel I.G., Ovcharenko O.I., Opanasyuk A.S., Gamernyk R.V., Furyer M.S. Stationary and time-resolved photoluminescence of nanostructured tin sulfide films. *Ukr. J. Phys.* **71**, No. 4, 331 (2026). https://doi.org/10.15407/ujpe71.4.331.

duced using cheap chemical methods [16–19]. These semiconductors are promising materials for the development of absorber layers in solar cells, near-infrared detector, anode material in lithium ion batteries, and semiconductor sensors [20–26].

SnS has p-type conductivity (the number of Sn vacancies is more than that of S vacancies [27–29]) and the orthorhombic symmetry. The interaction between the crystal layers is of the van der Waals type. This material is considered as very promising absorber layer for solar cells since its SCE is expected to be about 31% [30]. An obstacle to realizing its potential is the presence of impurity phases such as SnS_2, Sn_2S_3, Sn_3S_4 and Sn_4S_5 and other defects, which can significantly affect its electronic properties [31]. It should be noted that the crystalline SnS_2 and Sn_2S_3 have n-type conductivity. The band gaps of these compounds correspond to (1.08–1.70) eV for SnS, (1.82–2.41) eV for SnS_2, and (0.95–2.20) eV for Sn_2S_3, respectively [26]. The presence of impurity phases with different crystalline structures and the band-gap values induces deformation in the crystal lattice, which reduces the effectiveness of the applications of such materials. Thus, the detection of impurity phases and various types of defects is an important task related to the development of new efficient materials for solar energy.

Thus, in order to improve the physical parameters of the investigated films, it is necessary to study their energy structure, electronic properties, and crystal structure in detail. The latest studies were carried out by us recently [32, 33]. The purpose of this work is to study the absorption and photoluminescence properties of nanostructured SnS films with the aim of obtaining information about the nature of the electronic processes, including their kinetics associated with the presence of different crystalline phases and point defects.

2. Experimental Methods

The investigated SnS films were obtained by the polyol synthesis method in the medium of diethylene glycol (DEG). In this case, the $SnCl_2 \cdot 2H_2O$ salt and thiourea were separately dissolved in DEG, and then they were slowly mixed. The resulting mixture was heated to a temperature of 210 °C for 120 minutes. Then the resulting sediment was dried at 60 °C for 12 hours in air in a drying cabinet. SnS films were deposited on cleaned glass substrates by sputtering an ink based on a suspension of nanoparticles dispersed in distilled water. It was shown that the average size of the synthesized nanoparticles was 26–28 nm. The studied samples were deposited on glass substrates, their surface area was 20×20 mm^2, and the thickness was about 20 μm. This method is described in more detail in [33].

A DRON 4-07 X-ray diffractometer was used to study the structural properties of the investigated tin sulfide films. The obtained XRD pattern of tin sulphide films was normalized to the intensity of the (111) peak. Here, a Cu–K_α radiation source with $\lambda = 0.154050$ nm was used. The study of the morphology was carried out using an SEO-SEM Inspect S50-B scanning electron microscope.

A MAYA2000-pro spectrometer (Ocean Optics) was used for stationary photoluminescence studies. The PL spectra were excited by an LED with $\lambda = 274$ nm. PL decay measurements for different wavelengths were performed at room temperature using a LifeSpec II fluorescence spectrometer (Edinburgh Instruments) with time-correlated single photon counting (TCSPC) using an EPL405 type LED with $\lambda = 405$ nm and a pulse duration of 60 ps as the excitation source. It should be noted that the measurement of the PL kinetics was not carried out for a strictly fixed energy, but for a certain energy window, which is about 5 meV. A minimum peak power of the LED was 80 mW. The diameter of the illuminated surface of the sample was about 0.3 mm. The time interval between pulses was such that there was a complete attenuation of PL, i.e. a signal-to-noise ratio was measured.

The experimental data were fitted by a series of several hundred exponential functions combined with Non-Negative Truncated Singular Value Decomposition (NTSVD) technology. Such an algorithm does not require predefined shapes of the distributions and can effectively recover the lifetime distributions with multiple bands and peaks. It allowed us to determine the lifetime distributions associated with different recombination processes. In this case, we used a freeware demo version of the proprietary software Fluorescence Analysis Technology (FAST) developed by Edinburgh Instruments Ltd [34, 35]. This method is presented in more detail in our previous works [36, 37]. Photosensitivity spectra were measured using equipment based on the KSVU-23 spectrometer [38, 39].

3. Results and Discussion

3.1. Characterization of SnS films

Fig. 1 shows the SEM image of nanostructured SnS films obtained by spraying ink. According to the results presented in Fig. 1, the surface morphology of the films is porous and nanostructured [32].

Fig. 2 shows X-ray diffraction patterns of SnS films [32]. Diffraction reflections at angles of 30.8°, 39.3°, 44.0°, 68.8°, 73.2° correspond to planes (111), (131), (141), (081), (270) of orthorhombic SnS (JCPDS No. 14-0620). The most intense peak at an angle of 26.5° may originate from both the orthorhombic phase of SnS and the tetragonal phase of SnO_2, since according to the reference data of each compound, there is a corresponding plane at this angle. Peaks at angles of 50.4°, 55.5°, 59.8°, 70.3°, and 77.5° correspond to planes (110), (103), (112), (113), (203) of hexagonal SnS_2 (JCPDS No. 23-0677) and at angles of 54.7°, 57.7°, 62.8°, 64.8° correspond to planes (220), (002), (221), (112) of tetragonal SnO_2 (JCPDS No. 41-1445).

3.2. Absorption and photosensitivity spectra

The study of photoluminescence spectra of semiconductor nanostructured films requires data on the band structure and the nature of electronic processes which determine the structure of their optical spectra. This is especially important in the case of the presence of different crystalline phases, which is typical for the tin sulfide films we studied. In this case, the measurement of absorption spectra *along with photosensitivity spectra* is very useful to obtain the above-mentioned information. Therefore, this type of research on SnS films was carried out in this work.

Fig. 3, *a* shows the absorption spectrum (curve *1*) of the investigated films at room temperature. As can be seen from Fig. 3, *a*, the absorption spectrum has a strongly broadened edge that overlaps a wide spectral region from 1.0 eV to 3.5 eV. It should be noted that the shape of the absorption edge is not monotonic and has several spectral regions with different steepness. It is evident that the presence of these regions is due to various electronic processes, which can be associated with the presence of band-to-band optical transitions for different crystalline phases of tin sulphide films, including SnS, SnS_2 and Sn_2S_3 phases. Therefore, in addition, the absorption spectrum may contain spectral regions caused by different types of electronic transitions, which have different spectral dependences of the absorption coefficient. In this case, absorption due to optical transitions involving energy bands and energy levels of various defects can also be observed. The presence of these transitions causes the appearance of additional absorption, which significantly complicates the shape of the absorption edge.

It is well known that the band gap of semiconductor materials is usually determined by approximating

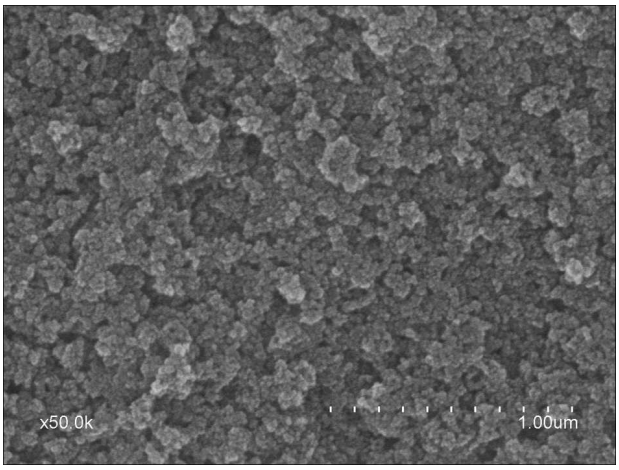

Fig. 1. SEM image of the surface of the nanostructured film obtained by the polyol synthesis method

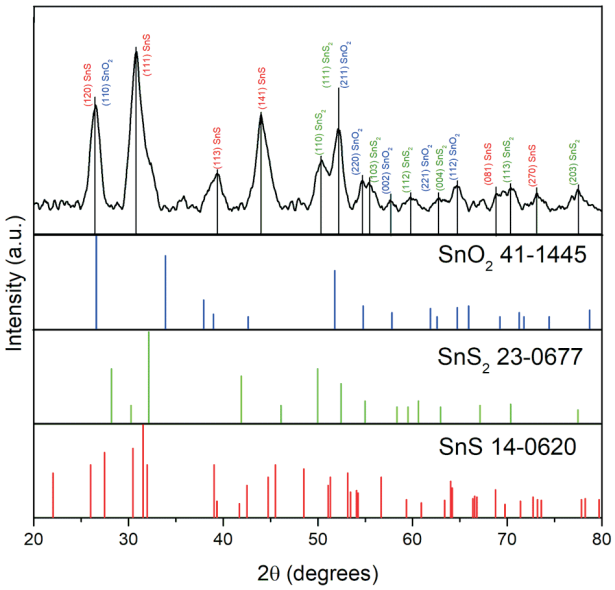

Fig. 2. XRD pattern of SnS films

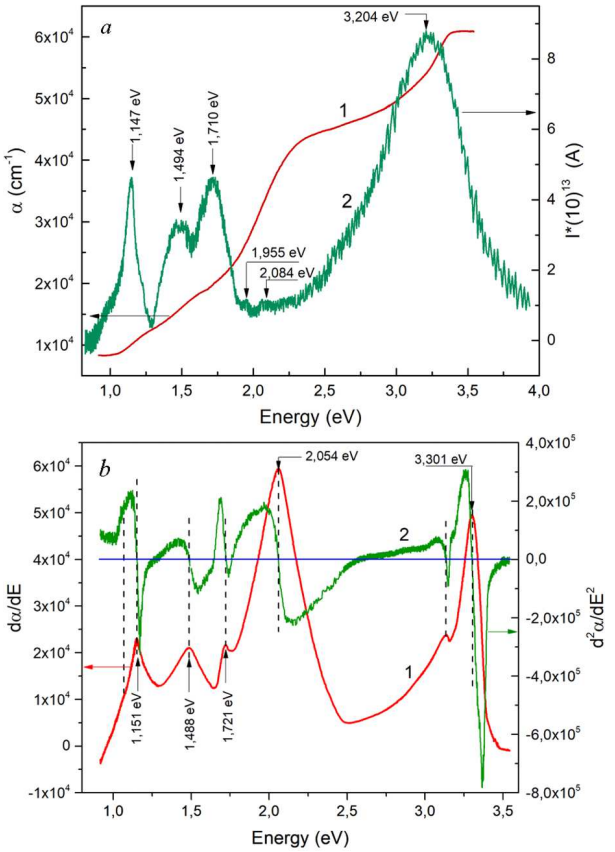

Fig. 3. Absorption (curve *1*) and photosensitivity (curve *2*) spectra of films at room temperature (*a*). ACFD (curve *1*) and ACSD (curve *2*) spectra of SnS films (*b*)

the absorption edge using the Tauc relation [40]. However, in our case, taking into account the complex shape of the absorption edge of the studied films, it is not possible to correctly perform such an approximation [41]. Earlier [42, 43], it was shown that an effective method of studying the nature of optical transitions associated with various electronic processes in semiconductor materials is the measurement of their photoelectric properties (photoconductivity or photodiffusion current spectra). This makes it possible to determine the energy of optical transitions, which are accompanied by the appearance of free charge carriers, namely, band-to-band transitions or transitions between energy bands and defect levels. Thus, in this case, we can obtain the value of the band gap as well as the ionization energy of defect levels and thus determine the type of crystalline phase and defects in the investigated materials.

As can be seen from Fig. 3, *a* (curve *2*), the photosensitivity spectrum shows a number of peaks at 1081 nm (1.147 eV), 830 nm (1.494 eV), 725 nm (1.710 eV), 634 nm (1.955 eV), 595 nm (2.084 eV) and 387 nm (3.204 eV) in the spectral regions that correspond to the absorption edge. According to [44–46], the appearance of the peak at 1.147 eV can be caused by band-to-band indirect allowed transitions of the SnS crystalline phase, since this energy is close to its band gap. At the same time, according to [47] and [48,49], the band gap of SnS in the case of the direct allowed transitions is 1.70 and 1.79 eV, respectively. Therefore, the peak at 1.710 eV can be associated with this type of optical transition in the SnS phase. Another peak at 1.494 eV may be the result of transitions between the defect level and the energy band. The ionization energy of this defect level corresponds to 216 meV. This can be attributed to the acceptor level, which determines the p-type conductivity of the SnS phase. The peaks at 2.084 eV and 1.955 eV may be caused by indirect forbidden transitions for another tin sulfide compound, namely SnS_2. In our opinion, such energies correspond to the band-to-band transitions and the transitions between the valence band and the donor level with the energy of 129 meV, which determines the n-type conductivity of the SnS_2 compound. The most intense line in the photosensitivity at 3.204 eV can be associated with the band-to-band direct allowed transitions of the SnO_2 compound.

3.3. ACFD and ACSD spectra

Additionally, in order to determine the band gap of different crystalline phases of the investigated SnS films, as well as, possibly, various defects, an analysis of the first and second derivatives of the absorption coefficient spectra, i.e., the ACFD and ACSD spectra, was performed. Earlier, the ACFD method was successfully used to determine the band gap in various semiconductor nanomaterials [50–52]. Fig. 3, *b* shows the ACFD spectrum of SnS films (curve *1*), which contains a number of peaks corresponding to the maximum values of the first derivative of the absorption coefficient with respect to the photon energy. They are located at the following energies: 1.151, 1.488, 1.721, 2.054 and 3.30 eV. The nature of these bands may be established by the comparison with the features of the absorption spectrum (see Fig. 3, *a*, curve *1*). In particular, the ACFD

band at 1.151 eV may correspond to the band-to-band transitions caused by indirect allowed transitions of the SnS compound. This correlates well with the values of the band gap obtained in the following works: (0.9–1.1) eV [53]; 1.08 eV [54]; 1.27 eV [55]. At the same time, the peculiarity at the long-wavelength edge of this band, located at 1.106 eV, may be evidently caused by direct optical transitions for the Sn_2S_3 compound. However, this additional structure in the ACFD spectrum can be caused by the presence of the defect in the SnS compound with the ionization energy of 91 meV, which must correspond to a shallow donor level in the SnS compound. However, this is unlikely, since this compound has p-type conductivity.

The ACFD band at 1.488 eV may correspond to that of direct allowed transitions of SnS, observed at 1.43 eV [56]. At the same time, the observed band at 1.721 eV is close to the values of 1,70 eV and 1.79 eV and can also be identified with this type of optical transitions [57–59]. We assume that the band at 1.488 eV is also caused by a similar type of optical transitions, including a defect level and one of the energy bands of SnS. The binding energy of such a defect level should be 233 meV. This is the acceptor level, which determines the p-type conductivity of this compound. Such a defect can be a tin vacancy (V_{Sn}), which is responsible for p-type conductivity and acts as a relatively deep level [60].

The ACFD band at 2.054 eV can be associated with the manifestation of indirect forbidden transitions of the SnS_2 compound. According to [45–47], the band gaps of these optical transitions correspond to 2.07, 2.2, and 2.41 eV, respectively. It should be noted that on the long-wavelength wing of the band at 2.054 eV, there is a feature in the form of a bend at an energy of 1.91 eV. The appearance of such a feature may indicate the possible manifestation of optical transitions in SnS_2, involving a shallow level with an energy of about 100 meV and one of the energy bands. In our opinion, this level can be a donor level, which is in good agreement with the n-type conductivity of SnS_2.

The ACFD spectrum also shows a band at 3.30 eV, which can be associated with the presence of an impurity phase SnO_2, which belongs to wide-band semiconductor materials ($E_g = 3.6$ eV). Thus, the appearance of this band can be caused by the absorption of a thin layer of SnO_2 formed on the surface of the SnS films.

In our opinion, the study of the spectra of the second derivative of the absorption coefficient is relevant, since in this case we hope to obtain more accurate information regarding the energy positions of the electronic transitions, as well as to determine the half-width of the ACFD bands. The last data allows us to obtain information regarding the homogeneity of the investigated materials, which is very important for the optimization of their crystal and optical quality during thermal annealing.

The ACSD spectrum of the investigated films is shown in Fig. 3, *b* (curve *2*). As can be seen from this figure, a feature of such a spectrum is that the maxima of the ACFD bands correspond to energy positions determined by the intersection of the spectral dependence of the second derivative of the absorption coefficient with the abscissa axis. This makes it possible to more accurately determine the energy of optical transitions associated with a certain type of electronic transition. The vertical lines shown in the figure confirm this. Thus, in the ACSD spectrum, a number of such crossings are observed at energies of 1.149, 1.488, 1.724, 2.058, 3.137, and 3.300 eV, which coincide with the maxima of the ACFD bands.

It should be noted that each ACFD band in the ACSD spectrum has a feature in the form of a dispersion curve, where the intersection with the abscissa axis determines the energy of electronic transitions, and the difference between the minimum on the short-wavelength side of the spectrum and the maximum on the long-wavelength side determines the half-width of the ACFD bands. The latter, as can be seen from Fig. 3 (curve *2*), correlates well with the photosensitivity bands of SnS films associated with a certain types of electronic transitions. Thus, these half-widths are obviously directly related to the crystalline and optical quality of the studied nanomaterials. It is important to note that in this case, the half-width of the band can be determined with sufficient accuracy even when it noticeable overlaps with other bands on the long- or short-wavelength edges. This is clearly seen for the ACFD bands at energies of 1.149 and 3.300 eV, where these values correspond to about 30 and 110 meV.

3.4. Stationary photoluminescence spectra

An effective method of studying the nature of electronic processes associated with the presence of various crystalline phases in tin sulfide films is also

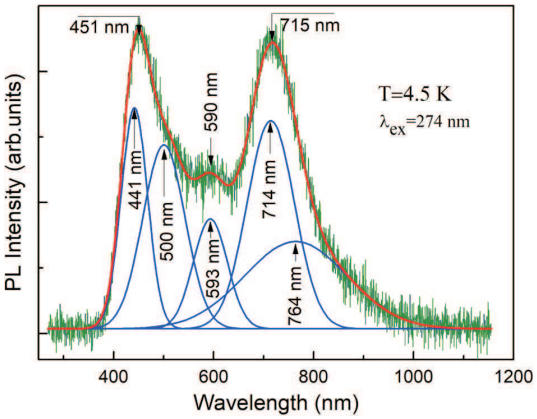

Fig. 4. Low-temperature photoluminescence of SnS thin films (sample 1)

the study of their low-temperature PL spectra [61–64]. The analysis of such spectra allows us to identify the presence of different crystal phases, since the energies of recombination processes will be different for them. At the same time, certain difficulties may arise, since in addition to optical transitions caused by band-to-band transitions, transitions involving the energy levels of defect states may also occur. Therefore, the PL bands of different nature can overlap, and this significantly complicates the analysis of the structure of low-temperature PL spectra. It should be noted that the study of PL spectra also makes it possible to obtain information about the homogeneity of the studied thin films, since the structure of the PL spectra is very sensitive to the presence of different crystal phases and structural defects.

Fig. 4 shows the low-temperature (4.5 K) PL spectrum of tin sulphide films. This spectrum corresponds to the central part (sample 1) of the investigated material (20×20 mm^2), which makes up more than 90% of its area.

Thus, the shape of the PL spectrum is the same for the main part of the surface of the studied samples, which indicates the high homogeneity of such films. However, as will be shown below, the shape of the PL spectrum is noticeably different at the edges of the sample under study. PL excitation was carried out by an LED with a wavelength of 274 nm. Here, three PL bands at 451 nm (2.75 eV), 590 nm (2.10 eV) and 715 nm (1.73 eV) are observed. Earlier, the PL band at 720 nm was observed in [65], which is caused by band-to-band transitions. According to the XRD results, the investigated films, in addition to the main SnS phase, also contain other phases (SnS_2 and SnO_2). Therefore, the structure of the PL spectrum may be caused by the presence of different crystalline phases in the investigated films. As can be seen from Fig. 4, the shortest-wavelength PL band at 451 nm cannot be identified with any crystalline phase of tin sulphide, since its energy position significantly exceeds their band gap values. Therefore, this PL band is obviously due to the presence of the SnO_2 phase. As was shown in [65], SnO_2 films exhibit the PL peaks at 371 nm and 430 nm that are associated with some near band edge emission and the surface defects of SnO_2 nanoparticles, respectively. It was shown that the emission of the PL band at 430 nm depends on the shape of nanoparticles [66]. It should be noted that small SnO_2 nanoparticles have a lot of defects, such as oxygen vacancies, due to their large surface area. Therefore, the PL intensity of this band should increase with decreasing nanoparticle size. PL measurements of SnO_2 nanoparticles were also performed in [66], where the bands at 470 nm and 480 nm were observed. These bands are associated with the emission from shallow and deep trap states.

As can be seen from Fig. 4, the deconvolution of the PL spectrum shows the presence of five components at 441 nm (2.81 eV), 500 nm (2.48 eV), 593 nm (2.09 eV), 714 nm (1.73 eV), and 764 nm (1.62 eV). In our opinion, the appearance of PL bands at 441 nm and 500 nm can be associated with participation in the process of recombination of the defects in the volume and on the surface of SnO_2 nanoparticles, respectively. In [67] two bands of strong intensity were observed at 549 nm and 700 nm for SnS_2 with a band gap of about 2.2 eV, which the authors explain as being due to the following mechanisms: recombination processes involving intrinsic defects, bound excitons, defects caused by stresses in the films, and impurity states. It is obvious that the PL band at 593 nm is due to the SnS_2 phase. At the same time, the band at 714 nm can be associated with the presence of SnS phase, which corresponds to the direct allowed transitions [65]. This result also correlates with the data of the absorption and photoconductivity measurements. Another band at 764 nm, also associated with this type of optical transition, may be due to the emission involving a shallow defect level with the ionization energy of about 100 meV.

Fig. 5 shows the low-temperature PL spectrum of tin sulfide films (sample 2). In this case, the emis-

sion was measured approximately 3 mm from the edge of the investigated SnS sample. As can be seen from Fig. 5, the deconvolution of the PL spectrum observed seven components at 417 nm (2.97 eV), 447 nm (2.80 eV), 495 nm (2.50 eV), 591 nm (2.10 eV), 721 nm (1.72 eV), 878 nm (1.41 eV), 995 nm (1.25 eV). Here, the short-wavelength region of the PL spectrum contains three components at 417 nm, 447 nm, and 495 nm. This indicates that in this case, the recombination processes involving three defect levels with different ionization energies occur in SnO_2 nanoparticles. Two additional PL bands at 591 nm and 721 nm are due to the recombination processes associated with the band-to-band optical transitions in the SnS_2 and SnS phases, respectively. At the same time, the PL band at 878 nm is obviously due to similar optical transitions involving a defect level previously observed in the photosensitivity spectrum. The appearance of the PL band at 995 nm may be associated with the indirect band-to-band transitions in the SnS phase.

Thus, the analysis of the structure of the PL spectra indicates that the obtained tin sulfide films for samples 1 and 2 are homogeneous with respect to the presence of different crystalline phases. However, the amount of their intrinsic structural defects is different. For the samples obtained near the edge of the deposited films (sample 2), the number of such defects increases noticeably.

Fig. 6 shows the PL spectrum of nanostructured SnS films at helium temperatures obtained using optical excitation at 395 nm, where a rather narrow band at 1196 nm (1.037 eV) was detected. Considering that the band gap for the impurity secondary phase Sn_2S_3 is about 1.0 eV, it can be assumed that such a band is due to recombination processes involving the energy bands of this compound or to the emission of exciton states.

3.5. PL kinetics and its analysis

The time-resolved study of the photoluminescence of nanostructured semiconductor films allows us to obtain important information about the time evolution of different electronic recombination processes, i.e. the peculiarities of their electronic properties, which determine the response speed of devices developed on the basis of the investigated materials. It should be noted that the lifetimes of different electronic processes depend on the presence of intrinsic

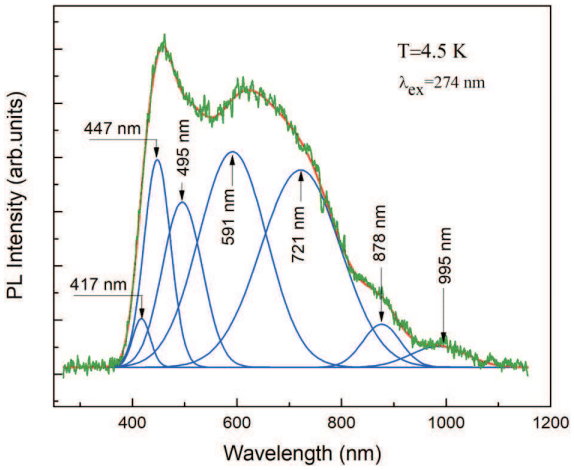

Fig. 5. Low-temperature (4.5 K) photoluminescence spectrum of tin sulphide films (sample 2)

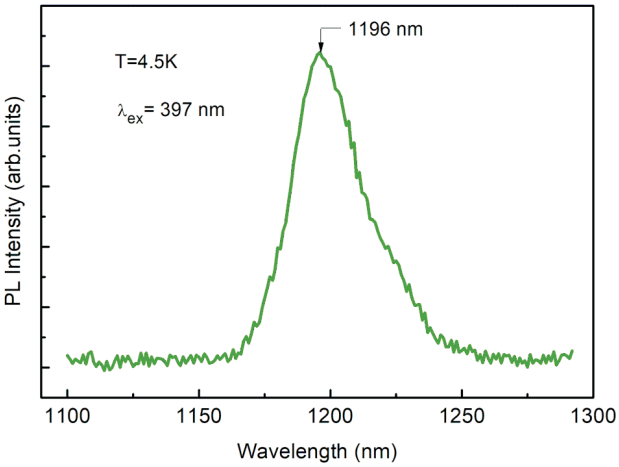

Fig. 6. Low-temperature photoluminescence of SnS films excited by 395 nm

and extrinsic defects in such materials as well as secondary crystalline phases.

Studying photoluminescence kinetics allows us to obtain information about the time evolution of the PL spectral bands [38] and their decay times [36, 37], which is very useful for establishing the nature of the electronic processes and the response speed of the investigated nanostructured materials that determine the effectiveness of their application. In this case, we can obtain an average lifetime as well as the lifetime distribution. The analysis of the obtained results made it possible to study the nature of the different defects and their effect on the electronic processes in detail.

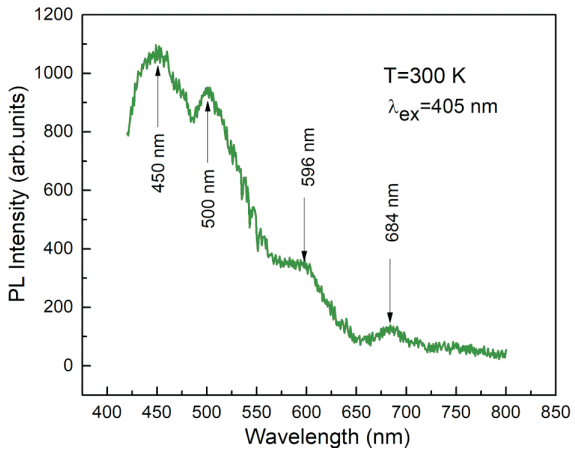

Fig. 7. Photoluminescence spectrum of SnS film at room temperature

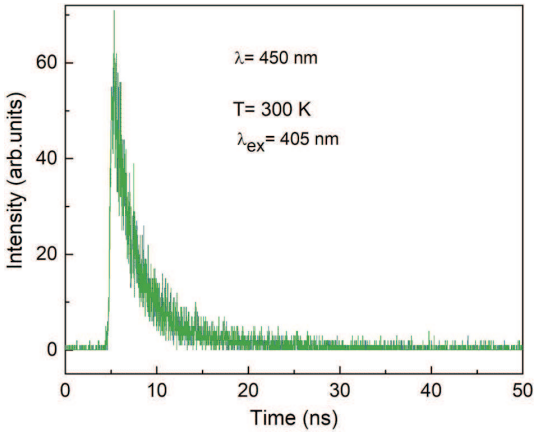

Fig. 8. Experimental kinetics of the PL band at 450 nm in SnS nanoparticles under excitation by a pulsed laser with a wavelength of 405 nm

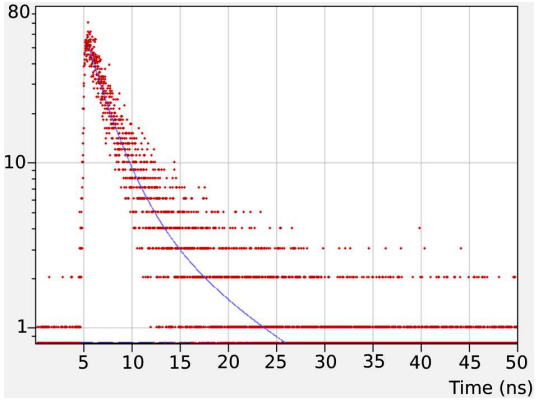

Fig. 9. PL decay kinetics of SnS nanoparticles at room temperature at a wavelength of 450 nm and its approximation by a sum of 200 exponential components

In this work, we conducted a study of the kinetics of PL spectral bands for nanostructured SnS films. Such studies made it possible to determine the lifetimes for various recombination processes and thus obtain additional information about their nature associated with a certain type of optical transitions, which is determined by the energy of such optical transitions. Fig. 7 shows the PL spectrum of SnS obtained at room temperature. It can be seen that this spectrum exhibits a structure corresponding to bands of strong intensity at 450 and 500 nm, as well as weaker bands at 596 and 684 nm. The sensitivity of this spectrometer made it possible to conduct a study of PL kinetics for PL bands at 450 and 596 nm.

Fig. 8 shows the experimentally obtained time dependence of PL decay for SnS nanoparticle films at the wavelength of 450 nm, which corresponds to the maximum of the shortest-wavelength PL band. It can be seen that the decay time mainly lies within the time interval up to 15 ns. Subsequently, the experimental results were fitted not by a single exponent or the sum of two exponents, as is usually done in the literature, but instead, we performed the photoluminescence decay kinetics analysis using a non-parametric lifetime distribution reconstruction approach based on reconvolution and non-negative least-squares fitting. The procedure enables the extraction of complex multi-exponential decay components without assuming a predefined kinetic model, making it suitable for systems exhibiting dispersive or strongly heterogeneous recombination dynamics. The analysis performs reconvolution with a logarithmically spaced basis of exponential kernels, alongside amplitude recovery using projected-gradient non-negative least squares (PG-NNLS) approach. This makes it possible to effectively fit experimental data by a series of several hundred (we used 200) exponential components with fixed τ_i evenly distributed on a logarithmic scale. $I(t) = \sum_{i=1}^{N} F_{\tau_i} e^{-\frac{t}{\tau_i}}$ and recover the distribution of the amplitudes F_{τ_i} (lifetime distribution).

This approach was previously proposed and used by us in [36, 37]. In this case, as a result of such analysis, not the average lifetime over the ensemble of nanoparticles, but the distribution of lifetimes for various recombination processes is obtained.

Fig. 9 shows such an analysis of the experimentally obtained PL decay using the method described above. Fig. 10 shows the recovered distribution of lifetimes for recombination processes that occur for

a wavelength of 450 nm with an energy window of 5 meV.

As can be seen from Fig. 10, the distribution of the lifetimes of recombination processes has two relatively broad maxima in the nanosecond range at 1.707 ns and 8.676 ns. It should be noted that, as follows from Table 1, the contribution of the first distribution band is decisive and amounts to 93.46%. The half-width of such a band is about 2 ns, i.e., taking into account the value of the maximum of the distribution, it is quite significant.

As previously shown in the measurement of PL spectra of nanostructured SnS films at $T = 4.5$ K, the emission band at 450 nm is due to recombination processes for the secondary SnO_2 phase with the participation of surface states, which appear on the surfaces of the synthesized nanoparticles of different sizes.

For such nanoparticles, there will be a certain distribution of the magnitude of the "stretchiness" of the surface states, which is determined by the size of the nanoparticles. The presence of such a distribution in surface states leads to the manifestation of a corresponding distribution of the lifetimes of the corresponding recombination processes. It should be noted that the energy of such recombination processes does not differ much, i.e., it is within the energy window of the measurement data (about 5 meV).

Table 1. **Parameters obtained from fitting the PL decay curve at $\lambda = 450$ nm**

Peak num.	f (%)	τ (ns)	T (ns)
1	93.46	1.707	1.758
2	6.5396	8.676	8.540

Table 2. **Parameters obtained from fitting the PL decay curve at $\lambda = 596$ nm**

Peak num.	f (%)	τ (ns)	T (ns)
1	8.0e-6	0.013	0.012
2	88.68	2.329	2.257
3	11.32	13.815	13.493

Note: f is the band contribution of the band to the total PL (area fraction), τ is the peak position weighted by area (band centroid) and T is the peak position by height (τ at max intensity)

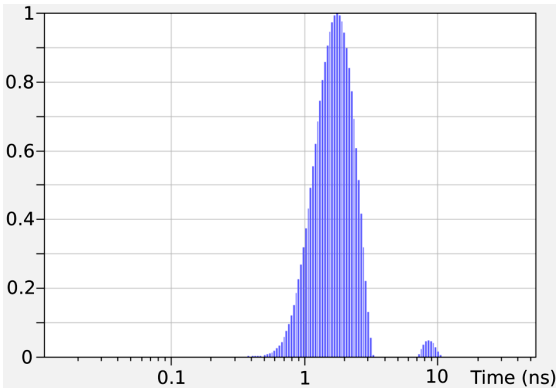

Fig. 10. Distribution of recombination lifetimes for SnS nanoparticles at the wavelength of 450 nm (2.75 eV) with an energy window of 5 meV

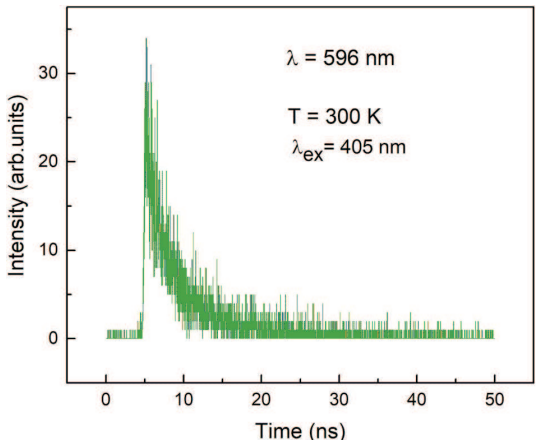

Fig. 11. PL decay kinetics of SnS nanoparticles at room temperature for the wavelength of 596 nm

Fig. 11 presents the experimental PL decay at 596 nm, which corresponds to the maximum of another intense band. The PL decay kinetics analysis and recovered lifetime distribution for recombination processes occurring at a wavelength of 596 nm are presented in Fig. 12 and Fig. 13, respectively. The parameters obtained as a result of the analysis of the experimental PL decay are given in Table 2. The obtained results indicate that three maxima in the lifetime distribution are theoretically expected. However, the contribution of the distribution band in the subnanosecond range is practically equal to zero. The largest contribution is made by the lifetime distribution band with a maximum at 2.257 ns (88.68%), and another maximum at 13.493 is about 11.32%.

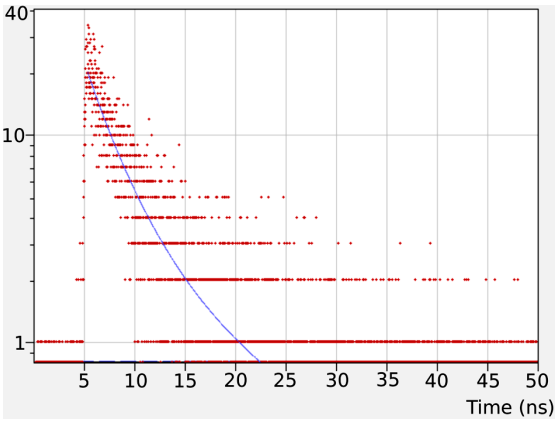

Fig. 12. PL decay kinetics of SnS nanoparticles at room temperature at a wavelength of 596 nm and its approximation by a sum of 200 exponential components

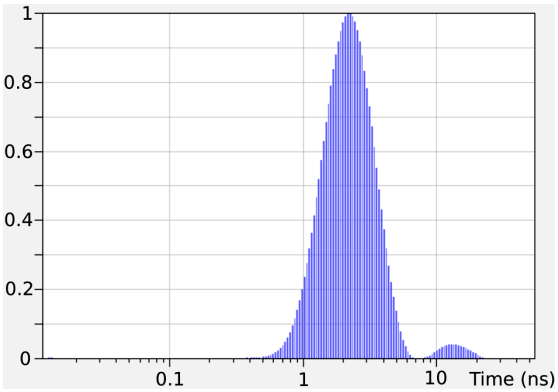

Fig. 13. Distribution of recombination lifetimes for SnS nanoparticles at the wavelength of 596 nm (2.08 eV) with an energy window of 5 meV

In fact, the qualitative distribution of lifetimes at wavelengths of 450 and 596 nm is similar. The difference is that at 596 nm, the maxima of the lifetime distribution are slightly shifted towards longer lifetimes. This may indicate that for the SnS_2 compound, the studied ensemble of nanoparticles has two separate subensembles of nanoparticles with different average sizes. Moreover, in each set, there is still a small dispersion in nanoparticle size of such nanoparticles, which leads to a certain dispersion in the distribution of the lifetimes of the recombination processes associated with such nanoparticles.

4. Conclusions

In this work, absorption and photosensitivity spectra, as well as stationary photoluminescence and their kinetics of thick (about 30 μm) nanostructured SnS films were investigated. These films were obtained by spraying ink made from a nanoparticle suspension onto glass substrates. They have the orthorhombic SnS phase, and the average sizes of the nanoparticles nanoparticle size is about 20 nm. Such films contain a small quantity of unwanted SnS_2, SnO_2, and, possibly, Sn_2S_3 phases.

Using the results of absorption studies and analysis of their ACFD and ACSD spectra, band-gap values of various crystalline SnS phases, as well as the SnO_2 phase, were determined. It was shown that the ACSD method makes it possible to more accurately determine the energy of optical transitions associated with a specific electronic transitions. At the same time, the half-width of the ACSD band allows us to determine the band-gap values with high accuracy as well as to obtain information regarding the homogeneity of the investigated materials. It was shown that the structure of the photoluminescence of the investigated films can be caused by the presence of different crystalline phases in the investigated films as well as different defects, the energy ionization of which was also determined.

Time-resolved photoluminescence studies of nanostructured SnS films revealed complex, multicomponent recombination dynamics characterized by broad lifetime distributions associated with heterogeneous recombination channels. For the PL band at 450 nm, the recombination is dominated by a short-lived component ($\sim$1.7 ns) with a minor longer-lived contribution, consistent with surface-state-mediated recombination in a secondary SnO_2 phase. A similar behavior is observed at 596 nm, although the characteristic lifetimes are shifted toward longer values, indicating size-dependent effects within distinct nanoparticle sub-ensembles. These results demonstrate that lifetime distribution analysis provides detailed insight into defect-related and surface-state recombination processes and is essential for understanding and optimizing the optoelectronic response of SnS-based nanostructured materials.

It is shown that the lifetimes of excited states in the studied films are in the nanosecond range.

Therefore, nanostructured SnS films are effective fast-acting materials suitable for creating environmentally friendly absorber layers in solar cells.

1. M.A. Green, E.D. Dunlop, M. Yoshita, N. Kopidakis, K. Bothe, G. Siefer, X. Hao, J.Y. Jiang. Solar cell efficiency tables (Version 66). *Progress in Photovoltaics: Res. Appl.* **33**, 795 (2025).
2. https://www.longi.com/en/news/.
3. B.M. Kayes, H. Nie, R. Twist *et al.* 27.6% conversion efficiency, a new record for single-junction solar cells under 1 sun illumination. In: *Proceedings of the 37th IEEE Photovoltaic Specialists Conference* (2011).
4. M. Nakamura, K. Yamaguchi, Y. Kimoto, Y. Yasaki, T. Kato, H. Sugimoto. Cd-free Cu (In, Ga)(Se, S)2 thin-film solar cell with a new world record efficacy of 23.35%. In: *46th IEEE PVSC, Chicago, IL*, June 19, 2019 (see also http://www.solar-frontier.com/eng/news/2019/0117_press.html).
5. M.J. Keevers, T.L. Young, U. Schubert, M.A. Green. 10% efficient CSG minimodules. In: *22nd European Photovoltaic Solar Energy Conference, Milan* (2007).
6. L. Han, A. Fukui, Y. Chiba *et al.* Integrated dye-sensitized solar cell module with conversion efficiency of 8.2%. *Appl. Phys. Lett.* **94**, 013305 (2009).
7. L. Han, A. Fukui, Y. Chiba *et al.* Integrated dye-sensitized solar cell module with conversion efficiency of 8.2%. *Appl. Phys. Lett.* **94**, 013305 (2009).
8. J. Faisst, E. Jiang, S. Bogati *et al.* Organic solar cell with an active area >1 cm^2 achieving 15.8% certified efficiency using optimized VIS-NIR anti-reflection coating. *Solar RRL* **7**, 2300663 (2023).
9. S. Sohila, M. Rajalakshmi, Chanchal Ghosh, A.K. Arora, C. Muthamizhchelvan. Optical and Raman scattering studies on SnS nanoparticles. *J. Alloys and Compounds* **509**, 5843 (2011).
10. G.H. Yue, W.Wang, L.S. Wang, X. Wang, P.X. Yan, Y. Chen, D.L. Peng. The effect of anneal temperature on physical properties of SnS films. *J. Alloys and Compounds* **474**, 445 (2009).
11. Juran Kim, Jayeong Kim, Seokhyun Yoon, Jeong-yoon Kang, Chan Wook Jeon, William Jo. Single phase formation of sns competing with SnS_2 and Sn_2S_3 for photovoltaic applications: Optoelectronic characteristics of thin-film surfaces and interfaces. *J. Phys. Chem. C* **122** (6), 3523 (2018).
12. Yu. Kumagai, L.A. Burton, A. Walsh, F. Oba. Electronic structure and defect physics of tin sulfides: SnS, Sn_2S_3, and SnS_2. *Phys. Rev. Appl.* **6**, 014009 (2016).
13. Md A.M. Patwary, Md A.Hossain, B.C. Ghos, J. Chakrabarty, S.R. Haque, S.A. Rupa, J. Uddin, T. Tanaka. Copper oxide nanostructured thin films processed by SILAR for optoelectronic applications, *RSC Advances* **12**, 32853 (2022).
14. X. Han, L. Wang, H. Ling, Z. Ge, X. Lin, X. Dai, H. Chen. Critical review of thermochemical energy storage systems based on cobalt, manganese, and copper oxides. *Renewable and Sustainable Energy Reviews* **158**, 112076 (2022).
15. A.S. Zoolfaka, R.A. Rani, A.J. Morfa, A.P. O'Mullane, K. Kalantar-zadeh. Nanostructured copper oxide semiconductors: a perspective on materials, synthesis methods and applications, *J. Mater. Chem. C* **2**, 5247 (2014).
16. D. Cabrera-Germana, J.A. García-Valenzuelab, M. Cota-Leala, M. Martínez-Gila, R. Acevesd, M. Sotelo-Lerma. Detailed characterization of good-quality SnS thin films obtained by chemical solution deposition at different reaction temperatures. *Mater. Sci. Semicond. Process.* **89**, 131 (2019).
17. I. Ammar, A. Gassoumi, A. Akkari, F. Delpech, S. Ammar, N. Turki-Kamoun. Deposition of SnS thin films by chemical bath deposition method: Effect of surfactants. *Eur. Phys. J. Plus.* **134**, 505 (2019).
18. W. Shan, Z. Fu, M. Ma, Z. Liu, Z. Xue, J. Xu, F. Zhang, Yo. Li. Facile Chemical bath synthesis of sns nanosheets and their ethanol sensing properties. *Sens.* **19**, 2581 (2019).
19. E. Sutter, J. Wang, P. Sutter. Surface passivation by excess sulfur for controlled synthesis of large, Thin SnS flakes. *Chem. Mater.* **32** (18), 8034 (2020).
20. K.J. Yu, Z. Yan, M. Han, J.A. Rogers. Inorganic semiconducting materials for flexible and stretchable electronics. *npj Flexible Electronics* **1**, 4 (2017).
21. G. Qinglei, Di Zengfeng. *Inorganic Flexible Electronics: Materials, Strategies, and Applications*. Editor by Yongfeng Mei, Gaoshan Huang, Xiuling Li (Wiley, 2022).
22. S. Huang, Y. Liu, Y. Zhao, Z. Ren, C.F. Guo. Flexible Electronics: Stretchable electrodes and their future. *Adv. Funct. Mater.* **29**, 1805924 (2019).
23. P. Pramanik, P.K. Basu, S. Biswas. Preparation and characterization of chemically deposited tin(II) sulphide thin films. *Thin Solid Films* **150**, 269 (1987).
24. G. Valiukonis, D.A. Guseinova, G. Krivaite, A. Sileica. Optical spectra and energy band structure of layer-type $A^{IV}B^{VI}$ compounds. *Phys. Status Solidi B* **135**, 299 (1986).
25. T. Jiang, G.A. Ozin, A. Verma, R.L. Bedard, Adsorption and sensing properties of microporous layered tin sulfide materials. *J. Mater. Chem.* **7**, 1649 (1998).
26. L.A. Burton, D. Colombara, R.D. Abellon, F.C. Grozema, L.M. Peter, T.J. Savenije, G. Dennler, A. Walsh. Synthesis, characterization, and electronic structure of single crystal SnS, Sn_2S_3, and SnS_2. *Chem. Mater.* **25**, 4908 (2013).
27. Juran Kim, Jayeong Kim, Seokhyun Yoon, Jeong-yoon Kang, Chan Wook Jeon, William Jo. Single phase formation of SnS competing with SnS_2 and Sn_2S_3 for photovoltaic applications: Optoelectronic characteristics of thin-film surfaces and interfaces. *J. Phys. Chem. C* **122** (6), 3523 (2018).
28. Yu. Kumagai, L.A. Burton, A. Walsh, F. Oba. Electronic structure and defect physics of tin sulfides: SnS, Sn_2S_3, and SnS_2, *Phys. Rev. App.* **6**, 014009 (2016).
29. L.A. Burton, D. Colombara, R.D. Abellon, F.C. Grozema, L.M. Peter, T.J. Savenije, G. Dennler, A. Walsh. Synthesis, characterization, and electronic structure of single crystal SnS, Sn_2S_3, and SnS_2. *Chem. Mater.* **25**, 4908 (2013).

30. G.L. Arauujo, A. Marti. Absolute limiting efficiencies for photovoltaic energy conversion. *Sol. Energy Mater. Sol. Cells.* **33**, 213 (1994).
31. A.R. Garcia-Angelmo, R. Romano-Trujillo, J. Campos-Alvarez, O. Gomez-Daza, M.T.S. Nair, P.K. Nair. Thin film solar cell of SnS absorber with cubic crystalline structure. *Phys. Status Solidi A* **212** (10), 2332 (2015).
32. Yu.P. Gnatenko, A.P. Bukivskii, V.Yu. Yevdokymenko, A.S. Opanasyuk, P.M. Bukivskij, S.A. Iliash, I.G. Vertegel, O.I. Ovcharenko, R.V. Gamernyk. Optical and photoelectric properties of nanostructured SnS films obtained by spraying ink using a nanoparticle suspension. *Mater. Res. Express* **11** (12), 125002 (2024).
33. V. Yevdokymenko, R. Pshenychnyi, O. Dobrozhan, A. Opanasyuk, Yu. Gnatenko, P. Bukivskij, O. Klymov, V. Muñoz-Sanjosé. Structural, microstructural, and optical properties of SnS films deposited by spraying the nanoink with post-growth temperature treatment. *Appl. Phys. A* **130**, 593 (2024).
34. https://www.edinst.com/product/advanced-fast-software/.
35. *FAST Advanced Analysis of Fluorescence Kinetics* (Edinburgh Instruments Ltd, 2011).
36. A.P. Bukivskii, Yu.P. Gnatenko, Yu.P. Piryatinski. Photoluminescence lifetime studies of PbI_2 nanoclusters and microcrystallites in $Pb_{0.30}Cd_{0.70}I_2$ alloys. *J. Phys. Chem. Sol.* **120**, 147 (2018).
37. A.P. Bukivskii, Yu.P. Gnatenko. Study of the photoluminescence kinetics of heterogeneous nanostructured $Pb_{0.30}Cd_{0.70}I_2$ solid solutions. *Mater. Chem. Phys.* **199**, 577 (2017).
38. Yu.P. Gnatenko, P.M. Bukivskij, Yu.P. Piryatinski, A.P. Bukivskii, P.A. Skubenko, R.V. Gamernyk. Time-resolved photoluminescence spectroscopy of excitons in layered semiconductor PbI_2 nanoclusters. *J. Appl. Phys.* **112**, 093708 (2012).
39. A.P. Bukivskii, Yu.P. Gnatenko, P.M. Bukivskij, M.S. Furier, L.M. Tarakhan, R.V. Gamernyk. Photoluminescence and photoelectric properties of CdTe crystals doped with Mo. *Physica B: Condensed Matter.* **546**, 411737 (2020).
40. J. Tauc. Optical properties and electronic structure of amorphous Ge and Si. *Mater. Res. Bull.* **3**, 37 (1968).
41. Yu.P. Gnatenko, P.M. Bukivskij, M.S. Furier, A.P. Bukivskii, A.S. Opanasyuk. Temperature dependence of the band gap of high optical quality CdS: Dy thin films based on exciton spectra. *Mater. Res. Express* **5**, 125902 (2018).
42. Yu.P. Gnatenko, I.O. Faryna, P.M. Bukivskij, O.A. Shigiltchoff, R.V. Gamernyk, S.Yu. Paranchych, L.D. Paranchych. Optical and photoelectric properties of vanadium-doped $Cd_{1-x}Hg_xTe$ crystals. *J. Phys.: Condensed Matter* **14** (29), 7027 (2002).
43. Yu.P. Gnatenko, Yu.P. Piryatinski, R.V. Gamernyk, I.O. Faryna, P.M. Bukivskij, S.Yu. Paranchych, L.D. Paranchych. Elaboration of new uncooled detector materials highly sensitive in the near-IR region. *SPIE, Materials for Infrared Detectors III, V*, **5209**, 156 (2003).
44. Z. Zainal, M.Z. Hussein, A. Ghazali. Cathodic electrodeposition of SnS thin films from aqueous solution. *Sol. Energy Mater. Sol. Cells* **40**, 347 (1996).
45. W. Albers, C. Haas, H.J. Vink, J.D. Wasscher. Investigations on SnS. *J. Appl. Phys.* **32**, 2220 (1961).
46. S. Lopez, A. Ortiz. Spray pyrolysis deposition of Sn_xS_y thin films. *Semicond. Sci. Technol.* **9**, 2130 (1994).
47. O.E. Ogah, G. Zoppi, I. Forbes, R. Miles. Thermally evaporated thin films of SnS for application in solar cell devices. *Thin Solid Films* **517**, 2485 (2009).
48. M. Calixto-Rodriguez, H. Martinez, A. Sanchez-Juarez, J. Campos-Alvarez, A. Tiburcio-Silver, M. Calixto. Structural, optical, and electrical properties of tin sulfide thin films grown by spray pyrolysis. *Thin Solid Films* **517**, 2497 (2009).
49. A.J. Ragina, K.V. Murali, K.C. Preetha, K. Deepa, T.L. Remadevi. A study of optical parameters of tin sulphide thin films using the swanepoel method. In: *Optics: Phenomena, Materials, Devices, and Characterization 2011: International Conference on Light, AIP Conference Proceedings* **1391**, 752 (2011).
50. A. Voznyi, V. Kosyak, P. Onufrijevs, L. Grase, J. Vecstaudža, A. Opanasyuk, A. Medvid'. Laser-induced SnS_2-SnS phase transition and surface modification in SnS_2 thin films. *J. Alloys Compd.* **688**, 130 (2016).
51. L. Attou, B. Jaber, H. Ez-Zahraouy. Effect of annealing temperature on structural, optical and photocatalytic properties of CuO nanoparticles, *Mediterr. J. Chem.* **7** (5), 308 (2018).
52. A.E. Abdelrahman, W.M.M. Yunus, A.K. Arof. Optical properties of tin sulphide (SnS) thin film estimated from transmission spectra. *J. Non-Cryst. Solids.* **358**, 1447 (2012).
53. N.R. Mathews, C.C. García, I.Z. Torres. Effect of annealing on structural, optical and electrical properties of pulse electrodeposited tin sulfide films. *Mater. Sci. Semicond. Process.* **16**, 29 (2013).
54. M. Reghima, A. Akkari, C. Guasch, N. Turki-Kamoun. Structure. Surface morphology, and optical and electronic properties of annealed sns thin films obtained by CBD. *J. Electron. Mater.* **43**, 3138 (2014).
55. J. Xu, Y. Yang, Z. Xie. Effect of vacuum annealing on the properties of sputtered SnS thin films. *Chalcogenide Lett.* **11**, 485 (2014).
56. T. Gotoh. Control of carrier concentration in SnS films by annealing with S and Sn. *Phys. Status Solidi A* **213**, 1869 (2016).
57. P. Jain, P. Arun. Influence of grain Size on the Band-gap of Annealed SnS Thin Films. *Thin Solid Films* **548**, 241 (2013).
58. O.E. Ogah, K.R. Reddy, G. Zoppi, I. Forbes, R.W. Miles. Annealing studies and electrical properties of SnS-based solar cells. *Thin Solid Films* **511**, 7425 (2011).
59. N. Revathi, S. Bereznev, M. Loorits, J. Raudoja, J. Lehner, J. Gurevits, R. Traksmaa, V, Mikli, E. Mellikov, O. Volo-

bujeva. Annealing effect for SnS thin films prepared by high-vacuum evaporation. *J. Vac. Sci. Technol. A.* **32**, 061506 (2014).
60. N.K. Samani, Z.D. Tafti, H.A. Bioki, M.B. Zarandi, S. Shayegh. Annealing effect on structural and optical constants of SnS thin films for solar cells application. *Optik.* **131**, 231 (2017).
61. Yu.P. Gnatenko, O.A. Shigil'chev, E. Rutkovskii, G. Contreras-Puente, M. Cardenas-Garcia. Photoluminescence and multiphonon resonant Raman scattering in Ni-and Co-doped $Zn_{1-x}Mn_xTe$ crystals. *Phys. Solid State* **40**, 564 (1998).
62. Yu.P. Gnatenko, A.S. Opanasyuk, M.M. Ivashchenko, P.M. Bukivskij, I.O. Faryna. Study of the correlation between structural and photoluminescence properties of CdSe thin films deposited by close-spaced vacuum sublimation. *Mater. Sci. Semicond. Proc.* **26**, 663 (2014).
63. Yu.S. Yeromenko, Yu.P. Gnatenko, A.S. Opanasyuk, D.I. Kurbatov, P.M. Bukivskij, M.S. Furier, V. Kuznetsov, A.P. Bukivskii. Photoluminescence of high optical quality CdS: Dy thin films deposited by close-spaced vacuum sublimation. *J. Luminescence*, **197**, 343 (2018).
64. A.P. Bukivskii, Yu.P. Gnatenko, Yu.P. Piryatinskii, R.V. Gamernyk. Nature of radiative recombination processes in layered semiconductor PbCdI2 nanostructural scintillation material. *J. Luminescence* **185**, 83 (2017).
65. M. Devika1, N. Koteeswara Reddy, M. Prashantha, K. Ramesh, S. Venkatramana Reddy, Y.B. Hahn, K.R. Gunasekhar. The physical properties of SnS filmsgrown on lattice-matched and amorphous substrates, *Phys. Status Solidi A* **207**, 1864 (2010).
66. Smritimala Sarmah, A. Kumaю Optical properties of SnO_2 nanoparticles. *Indian J. Phys* **84**, 1211 (2010).
67. N.G. Deshpande, A.A. Sagade, Y.G. Gudage, C.D. Lokhande. Ramphal Sharma, Growth and characterization of tin disulfide (SnS_2) thin film deposited by successive ionic layer adsorption and reaction (SILAR) technique. *J. Alloys and Compounds* **436**, 421 (2007).

Received 11.01.26

Ю.П. Гнатенко, А.П. Буківський,
П.М. Буківський, С.А. Іляш, І.Г. Вертегел,
О.І. Овчаренко, А.С. Опанасюк,
Р.В. Гамерник, М.С. Фур'ер

СТАЦІОНАРНА ТА РОЗДІЛЕНА В ЧАСІ ФОТОЛЮМІНЕСЦЕНЦІЯ НАНОСТРУКТУРОВАНИХ ПЛІВОК СУЛЬФІДУ ОЛОВА

В роботі досліджено оптичні властивості, включно зі спектрами фотолюмінесценції та їхньою кінетикою, товстих плівок SnS орторомбічної фази з низьким рівнем мікродеформації. Вони мають склад, близький до стехіометрії. Крім того, ці плівки містять невелику кількість інших кристалічних фаз, а саме: фаз SnS, SnS_2, SnO_2 та, імовірно, фази Sn_2S_3. Вивчення спектрів першої та другої похідних від коефіцієнта поглинання, тобто спектрів ACFD і ACSD, дало нам змогу точно визначити ширину забороненої зони різних кристалічних фаз. Аналіз спектрів ACSD також уможливив отримання інформації щодо однорідності досліджуваних наноматеріалів, що дуже важливо для оптимізації їхньої кристалічної й оптичної якості. Вивчення спектрів фотолюмінесценції дало нам змогу отримати інформацію про енергетичну структуру наноструктурованих плівок SnS, природу їхніх дефектів. На основі вимірювань кінетики затухання фотолюмінесценції було досліджено розподіли часу життя для різних процесів рекомбінації в SnS_2 і SnO_2. Такі дослідження дало змогу визначити час життя для різних процесів рекомбінації і таким чином отримати додаткову інформацію про їхню природу, пов'язану з певним типом оптичних переходів, яка визначається енергією таких переходів. Було показано, що час життя збуджених станів в досліджуваних плівках міститься в наносекундному діапазоні. Таким чином, отримані результати можуть допомогти в розробці нових швидкодійних ефективних наноматеріалів, придатних для створення на їхній основі екологічних абсорбуючих шарів для сонячних елементів.

Ключові слова: фотолюмінесценція, кінетика, заборонена зона, дефекти, фазовий стан, наноструктуровані плівки.